

Microhardness and Corrosion Resistance of Electrodeposited Ni–SiC–BN Composite Coatings

Xinyue Wang, Haoxuan Cui, Qian Zhou*, Xiliang Zhang, Yanru Zhang

School of Materials Science and Engineering, Hebei University of Engineering, Handan, 056038, China

*E-mail: dqianzhou@163.com

Received: 3 March 2022 / Accepted: 25 April 2022 / Published: 7 May 2022

Ni–SiC–BN composite coatings were electrodeposited on H13 steel in a Watt's bath with SiC and BN particles. The effects of SiC and BN concentration in the bath on the microstructure, microhardness and corrosion resistance of the composite coatings were investigated. The results revealed that the coating grains were refined by adding the concentration of SiC and BN particles. The content of these particles embedded in the composite coating increased until the particles concentration reached 37.5 g/L. Ni–SiC–BN composite coating exhibited the highest microhardness ($403.0 \pm 21.2 \text{ HV}_{0.2}$) when the particles concentration was 37.5 g/L, which was due to the superior dispersion strengthening, fine grain strengthening, high density dislocation strengthening and the supporting effect of high-hardness particles. The composite coating with the maximum capacitance arc radius and R_{ct} value ($2.518 \times 10^5 \Omega \cdot \text{cm}^2$) was obtained at 25 g/L, showing the highest corrosion resistance, which was attributed to the compact and uniform microstructure. And these particles that act as a barrier limited the exposed area of Ni matrix to the corrosive electrolyte.

Keywords: Electrodeposition, Ni–SiC–BN composite coatings, microstructure, microhardness, corrosion resistance.

1. INTRODUCTION

Electrodeposited Ni matrix composite coatings with excellent properties, such as high hardness, wear resistance and corrosion resistance, have been widely used in industrial applications, especially as a potential candidate for hard chromium coatings [1-3]. During electrodeposition process, second phase reinforcements suspended in a conventional Ni plating solution are adsorbed on the cathode surface under various driving forces. Then these reinforces are trapped and embedded in Ni matrix with the growing Ni layer. The resultant coating combining the advantages of the Ni matrix and reinforcements shows superior properties as compared to pure Ni coating. The combinations that have received

considerable attention are electrodeposited Ni with WC [4], Al₂O₃ [5,6], SiO₂ [7,8], TiC [9], SiC [10], CeO₂ [11,12], TiO₂ [13,14], CNTs [15] and BN [3], etc. For instance, the reinforcements such as TiO₂, CeO₂, or Al₂O₃ are preferred for improving the corrosion resistance of the coating. The microhardness and wear resistance of Ni matrix composite coatings can be increased by the incorporation of hard carbides, diamond, or solid lubricates.

Ni–SiC composite coating has been extensively studied by researchers [1,10,16]. They have mainly emphasized that the dispersion strengthening from second phase reinforcements was used to improve the mechanical properties of the composite coatings. Such the coating has large projected applications in aerospace, medical devices, marine, agriculture, or nuclear field, etc [17]. Ni–BN composite coating is interesting, owing to the considerably high surface microhardness, wear resistance and corrosion resistance [3,18]. In addition to dispersion strengthening, the incorporation of BN particles with self-lubricating nature can significantly reduce the friction coefficient and improve wear resistance of the coating. Shahri et al. [19] reported that BN with hexagonal close packed structure exhibits better performances than for other solid lubricants due to the weak bonding between layers caused by a little van der Waals forces. From what has been discussed above, the combined effect of SiC and BN particles on the mechanical properties and corrosion resistance of Ni matrix coating was proposed.

Previous study has demonstrated that the addition of SiC and BN particles can improve the microstructure and mechanical properties of Ni matrix coating, whereas it was restricted by the type and content of surfactant [20]. The effects of SiC and BN concentration on the coatings have yet to be clarified. In this work, Ni–SiC–BN composite coating was electrodeposited on H13 steel in a typical Watt's bath containing SiC and BN particles. Then the effects of the particles concentration on the microstructure, microhardness and corrosion resistance of the composite coating were investigated.

2. EXPERIMENTAL

2.1 Materials and processes

H13 steel with dimensions of 20 mm × 15 mm × 3 mm was selected as the cathode and Ni plate was used as anode. Their area ratio was 1:2 and the distance was 2 cm. Before electrodeposition, each sample was mechanically polished to 1000-grit finish, followed by ultrasonic cleaned in anhydrous ethanol for 3 min and degreased in 10 wt.% sodium hydroxide for 15 min. Then the sample was activated in 5 wt.% hydrochloric acid solution for 1 min as the electrode.

Pure Ni coating was prepared by electrodeposition from a typical Watt's bath. The detailed electroplating process was as follows: NiSO₄·6H₂O 240 g/L, NiCl₂·6H₂O 40 g/L, SDS 0.15 g/L, NH₄Cl 40 g/L, H₃BO₃ 40 g/L, pH 5.0, temperature 50 °C, current density 4 A/dm², plating time 60 min and stirring speed 500 rpm. After adding SiC and BN particles to the Watt's bath, Ni–SiC–BN composite coatings were obtained, and other processes were the same as those of pure Ni coating. The total concentrations of SiC and BN particles were 12.5 g/L, 25 g/L, 37.5 g/L or 50 g/L, with their mass ratio being 1:1 in the bath. The resultant composite coatings were successively recorded as Ni–12.5 g/L SiC/BN, Ni–25 g/L SiC/BN, Ni–37.5 g/L SiC/BN or Ni–50 g/L SiC/BN. The size of received SiC particle with lumpy structure was about ~700 nm, and the size of received BN particle with flattened spheroid structure was about ~300 nm. Before deposition, these particles were ultrasonically dispersed

for 24 h to prevent agglomeration. The plating process was carried out in a 400 ml beaker placed in a constant temperature magnetic stirrer.

2.2 Characterization

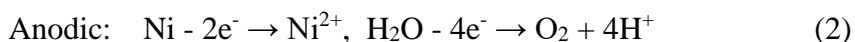
The surface morphology of the coating was observed by a scanning electron microscopy (SEM). An energy dispersive spectrometer (EDS) was applied to detect the composition of the coatings. The structure of the coating was characterized using an X-ray diffractometer (XRD) with Cu K α generated at 40 kV and 40 mA, and the grain sizes in the corresponding crystallographic planes were calculated according to Scherrer equation.

Vickers microhardness tester was applied to measure the microhardness of the coating under the load of 200 g for 15 s. Corrosion behaviors were measured by a VersaSTAT3 electrochemical system in 3.5 wt.% NaCl solution. A traditional three electrode system was performed, within the coating with an area of 1 cm² as working electrode. The reference electrode and counter electrode were the saturated calomel electrode (SCE) and platinum plate, respectively. To obtain a stable open circuit potential, the electrochemical impedance spectra (EIS) measurements were conducted after immersing the samples for 0.5 h. The testing frequency range was determined to be 100 kHz to 10 mHz. The applied sinusoidal potential amplitude was 10 mV. The coating pore resistance (R_c) and charge transfer resistance (R_{ct}) were used to evaluate the corrosion resistance.

3. RESULTS AND DISCUSSION

3.1 Deposition of Ni–SiC–BN composite coating

The electrodeposition process of Ni–SiC–BN composite coating is similar to that of pure Ni deposition, which can be characterized by the cathode and anode reactions. The Ni ions (Ni²⁺) near the cathode were reduced into Ni metal by gaining electrons, which was accompanied with the side reaction of hydrogen evolution. The Ni plate as an anode loses electrons to form Ni²⁺ to compensate for the loss of Ni²⁺ in the bath. In addition, oxygen evolution as a side reaction occurs on the anode surface. The detail reactions are shown below.



The difference is that the cathode process of the composite coating involves the incorporation of SiC and BN particles. Previous works [21,22] indicated the electrodeposition process of these dispersed particles can be described in three steps. Firstly, these dispersed particles suspended in the bath move toward the cathode under the mechanical agitation, electric field or diffusion. Secondly, these particles are adhered on the cathode surface. Finally, these particles are trapped by the growing Ni layer to form a composite coating. The schematic diagram demonstrated the electrodeposition process of Ni–SiC–BN composite coating is shown in Fig. 1.

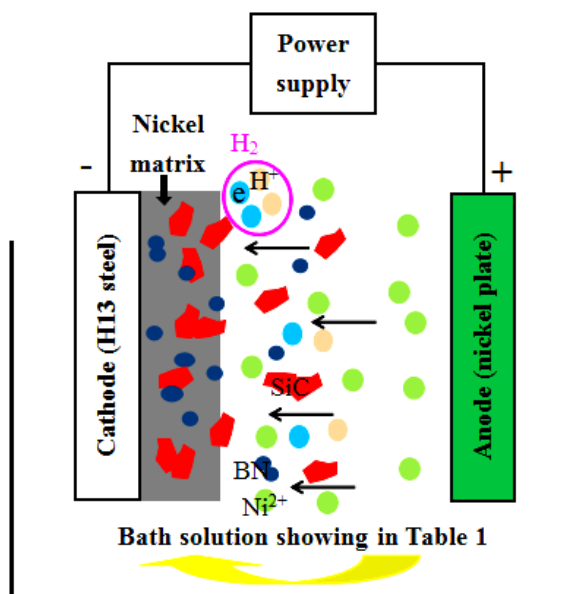


Figure 1. Schematic diagram demonstrated the electrodeposition process of Ni–SiC–BN composite coating.

Fig. 2 shows the cross-section morphology and EDS spectrum of the composite coating deposited in the bath with 37.5 g/L SiC and BN particles. From Fig. 2, the SiC and BN particles were successfully deposited in Ni matrix under the current process, indicating the formation of Ni–SiC–BN composite coating. The SiC and BN particles were uniformly dispersed in the Ni matrix coating, which was beneficial to improve the properties of the coating.

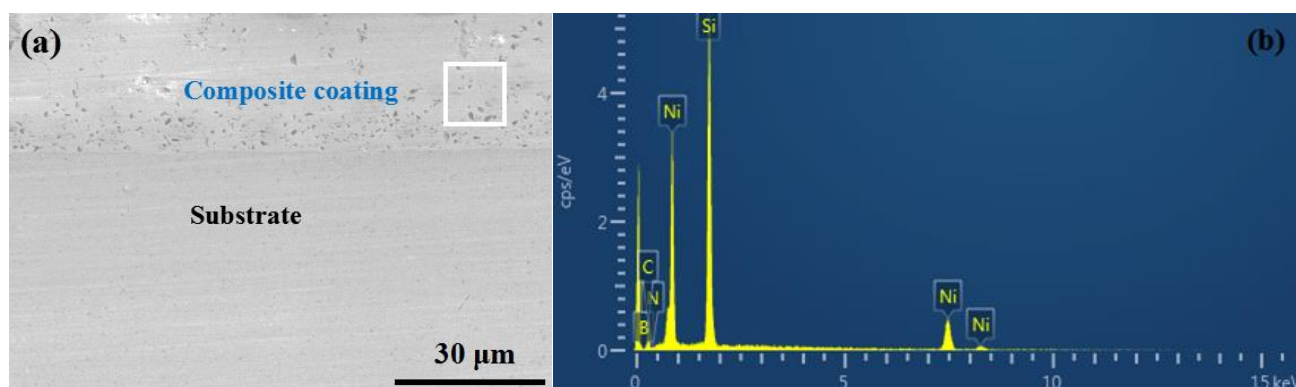


Figure 2. The cross-section morphology (a) and EDS spectrum (b) of the composite coating deposited in the bath with 37.5 g/L SiC and BN particles.

3.2 Microstructure

Fig. 3 shows the morphologies of pure Ni and Ni–SiC–BN composite coatings. From Fig. 3(a), the cauliflower-like pure Ni coating was observed. After adding SiC and BN particles to the bath, these particles were embedded into the Ni matrix as the plating process proceeded. As a result, the different degrees of cellular bulges occurred on the surface of the composite coatings. The cellular bulges increased with the increase of SiC and BN particles. A minimal amount of lumpy SiC and spheroid BN

particles were embedded on the composite coating deposited in the bath with 12.5 g/L SiC and BN particles. When the particles were increased to 25 g/L or 37.5 g/L, a large number of SiC and BN particles were dispersed on the surface of the composite coating (Figs. 3(b) and (c)). However, the surface roughness of the composite coating was increased, which may be because too many particles in the bath led to the increase of cellular bulges caused by nucleation of SiC and BN particles. Indeed, a tip discharge effect occurs on the original cellular bulges. The Ni^{2+} was preferentially deposited on the original raised site, resulting in surface coarsening [23]. When the particles concentration was 50 g/L, some of particles agglomerate or precipitate at the bottom of the beaker, making them more difficult to be trapped. So that the content of these particles embedded in the coating decreased obviously, and the captured particles were displayed in a certain degree of agglomeration.

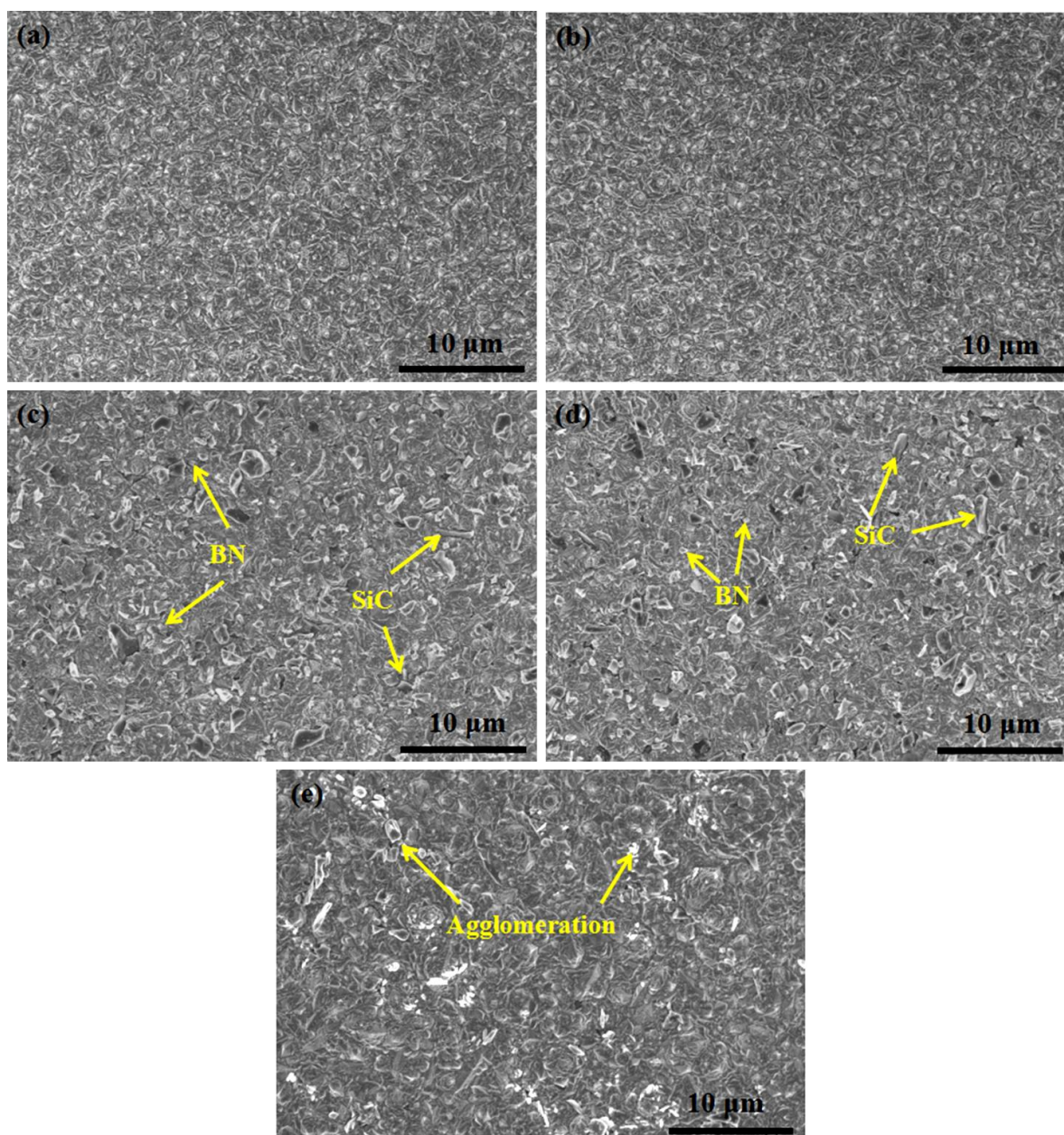


Figure 3. Morphologies of pure Ni (a) and Ni-SiC-BN composite coatings deposited in the bath containing SiC and BN particles of 12.5 (b), 25 (c), 37.5 (d) and 50 g/L (e).

Fig. 4 shows the XRD patterns of pure Ni and Ni–SiC–BN composite coatings deposited in the bath with 37.5 g/L SiC and BN particles. Five well-defined peaks representing Ni matrix were observed whether in pure Ni or the composite coating, which were correspond to the crystal planes (111), (200), (220), (311) and (222), respectively, suggesting a typical face-centered cubic structure. The diffraction peaks representing SiC and BN particles were detected in the composite coatings. This means that Ni–SiC–BN composite coating was obtained under the current electroplating process, which was consistent with the result shown in Fig. 2. Whereas, these diffraction peaks were almost invisible due to the low particles content embedded in composite coating. Afterward, the grain sizes of Ni matrix on all crystal planes in pure Ni and the composite coatings were calculated based on Scherrer equation, and the results are shown in Fig. 5. Compared with pure Ni coating, the Ni matrix grains on all crystal planes in the composite coating were refined when the particle concentration was 12.5 g/L. The cathodic polarization of the electrochemical reaction was enhanced by the addition of the second phase particles, and more nucleation sites for Ni matrix were provided. As a result, the nucleation rate of Ni matrix was accelerated while the growth rate was decreased [24,25]. However, the grain size of Ni matrix was increased gradually with the increase of the particles in the bath. The grain refinement effect was weakened. The grain sizes of the composite coating were larger than those of pure Ni coating when the particles concentration reached 50 g/L, which may be caused by the agglomeration of SiC and BN particles (Fig. 3).

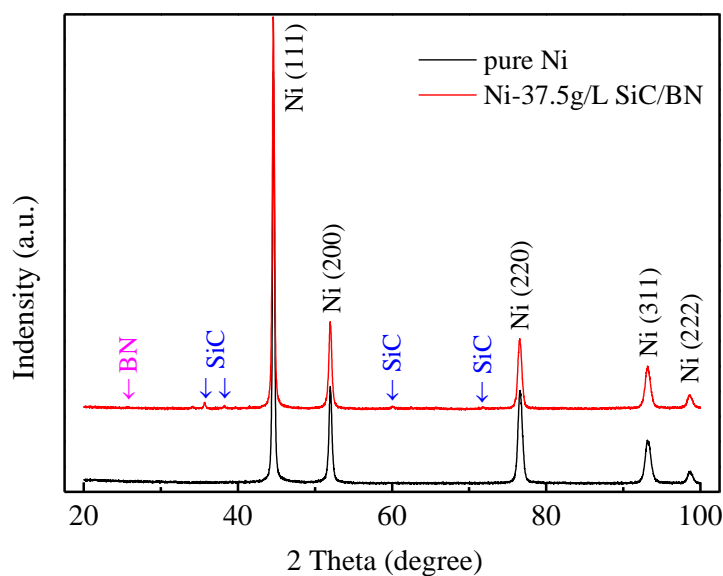


Figure 4. XRD patterns of pure Ni and Ni–SiC–BN composite coatings deposited in the bath with 37.5 g/L SiC and BN particles.

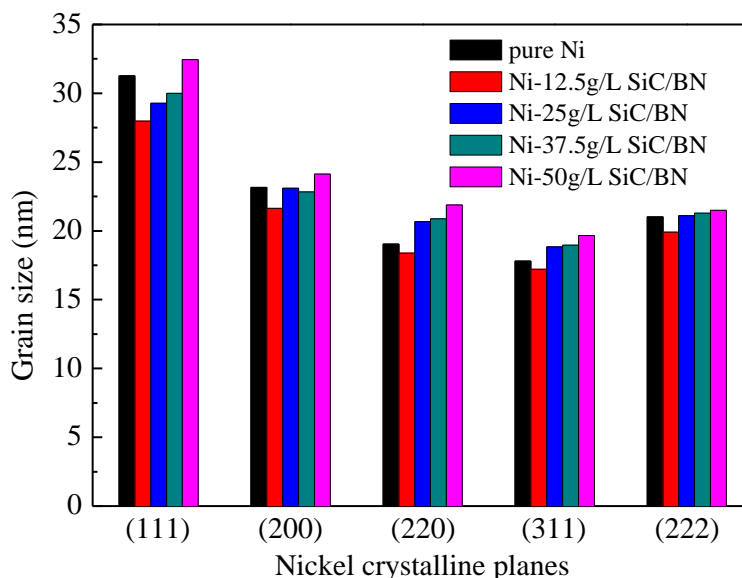


Figure 5. The grain sizes of the Ni matrix in pure Ni and Ni–SiC–BN composite coatings.

3.3 Microhardness

Fig. 6 shows the microhardness values of pure Ni and Ni–SiC–BN composite coatings deposited in the bath with various SiC and BN particles concentrations. As seen, adding the SiC and BN particles in the bath led to an increase in microhardness of the coatings. The maximum microhardness ($403.0 \pm 21.2 \text{ HV}_{0.2}$) was obtained at 37.5 g/L, which was approximately 20% higher than that of pure Ni coating ($336.4 \pm 7.1 \text{ HV}_{0.2}$). Four possible reasons for the enhanced microhardness of the composite coatings were discussed. The first is the grain refinement of Ni matrix. The corresponding strengthening mechanism was summed up as Hall-Petch relationship [26].

$$HV = 3\sigma_y \quad (3)$$

$$\sigma_y = \sigma_0 + kd^{-1/2} \quad (4)$$

where σ_y is the yield stress of Ni matrix, σ_0 is the friction stress, k is a constant, d is the grain size. Based on the equations, the microhardness of the coating is inversely proportional to its grain size. It can be interpreted as that the cathode polarization of the electrochemical reaction was increased by adding dispersed particles in the bath, resulting in a decreased in the grain size (Fig. 5). The increased grain boundary impeded the dislocation slip, improving the deformation resistance of the coating. So that the microhardness was increased. The second is dispersion strengthening effect described by Orowan mechanism [27].

$$\sigma = 2Gb / \lambda \quad (5)$$

where G is the shear modulus of Ni matrix, b is Burger's vector of the dislocation, λ is the distance of dispersed particles. Smaller distance of the dispersed particles caused by their higher content embedded in the coating was responsible for higher microhardness. The third is high density dislocation strengthening. The dislocation slip in Ni matrix was delayed or even hindered by dispersed particles embedded in the coating. As a result, severe distortion occurred in the Ni lattice near the dispersed particles. The dislocation strengthening effect on the composite coating was enhanced by the generated much internal stress. In addition, the supporting effect of the high-hardness particles on the coating was

also responsible for the increased microhardness. Further increasing the particles concentration to 50 g/L, the microhardness of the composite coating was decreased, which was attributed to the low content of dispersed particles embedded in the coating. The agglomeration of SiC and BN particles was also responsible for weakening reinforcement effect on the composite coating [28]. Indeed, the microhardness of Ni–SiC–BN composite coating in this study was directly related to the content of SiC and BN particles embedded in Ni matrix [29].

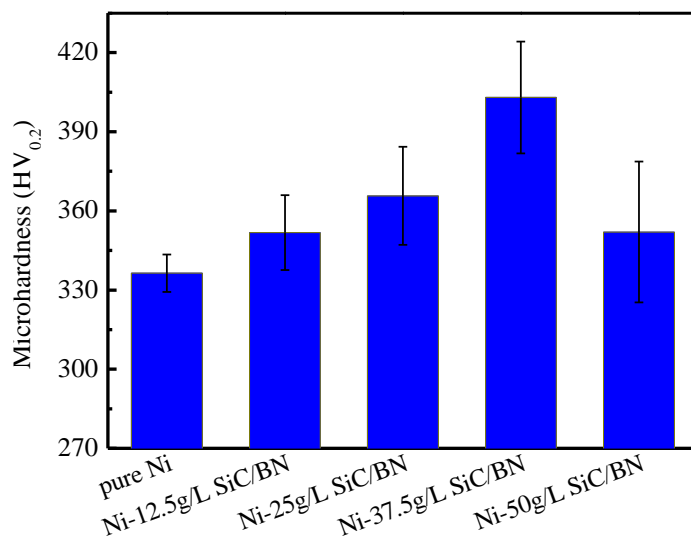


Figure 6. Microhardness values of pure Ni and Ni–SiC–BN composite coatings deposited in the bath with various SiC and BN particles concentrations.

3.4 Corrosion resistance

The EIS measurements were conducted in 3.5 wt.% NaCl solution. Fig. 7(a) shows the Nyquist plots of the coatings, and the corresponding impedance modulus and phase plots are shown in Figs. 7(b-c). From Fig. 7(a), the capacitive loop radius of Ni–SiC–BN composite coating was larger than that of pure Ni coating, and first increased and then decreased as SiC and BN particles in the bath increased. As the larger the radius of the capacitor ring, the better the corrosion resistance of the coating [23]. The maximum capacitance arc radius was observed in the composite coating deposited in the bath with 25 g/L particles, revealing the best corrosion resistance.

The defects (e.g. grain boundaries or phase boundaries) in the coating provided the direct diffusion path for the corrosive medium during testing. The galvanic corrosion cells were formed which dominate the corrosion process [4]. Two time constants were detected in Bode Plots (Figs. 7(b-c)). The time constant at the high frequency was attributed to the infiltration of electrolyte solution into the coating, and that at low frequencies was related to the interfacial reaction between the coating and steel matrix. Fig. 7(d) shows the corresponding equivalent circuit model, with EIS fitting results being provided in Table 1. R_s reveals the electrolytic solution resistance between the reference electrode and coated electrode. The similar R_s values ($9.148 \sim 11.40 \Omega \cdot \text{cm}^2$) were obtained in pure Ni and the composite coatings. R_c and Q_c are the coating pore resistance and constant phase element, which depend on the electrolyte/coating interface reactions and coating properties. R_{ct} and C_{dl} represent the charge

transfer resistance and double layer capacitance for the reaction at the electrolyte/substrate interface. As R_c and R_{ct} values were higher, the corrosion resistance of the coatings were stronger. From Table 1, R_c and R_{ct} values for the composite coating deposited in the bath with 12.5 g/L particles were increased slightly due to the compact and uniform microstructure [2]. The dispersed particles act as a barrier, limiting the exposed area of Ni matrix to the corrosive medium [30]. The corrosion resistance of the coating was increased. The R_c value was decreased as the particles in the bath increased, which may be due to the increased interfaces caused by the incorporation of SiC and BN particles providing the direct diffusion path for the corrosive medium. R_{ct} value was increased due to the barrier effect of the insulating particles. The maximum R_{ct} value ($2.518 \times 10^5 \Omega \cdot \text{cm}^2$) was obtained at the particles concentration of 25 g/L. In this case, the composite coating showed the highest corrosion resistance. Further increasing the particles concentration in the bath, the corrosion resistance of the composite coating was deteriorated.

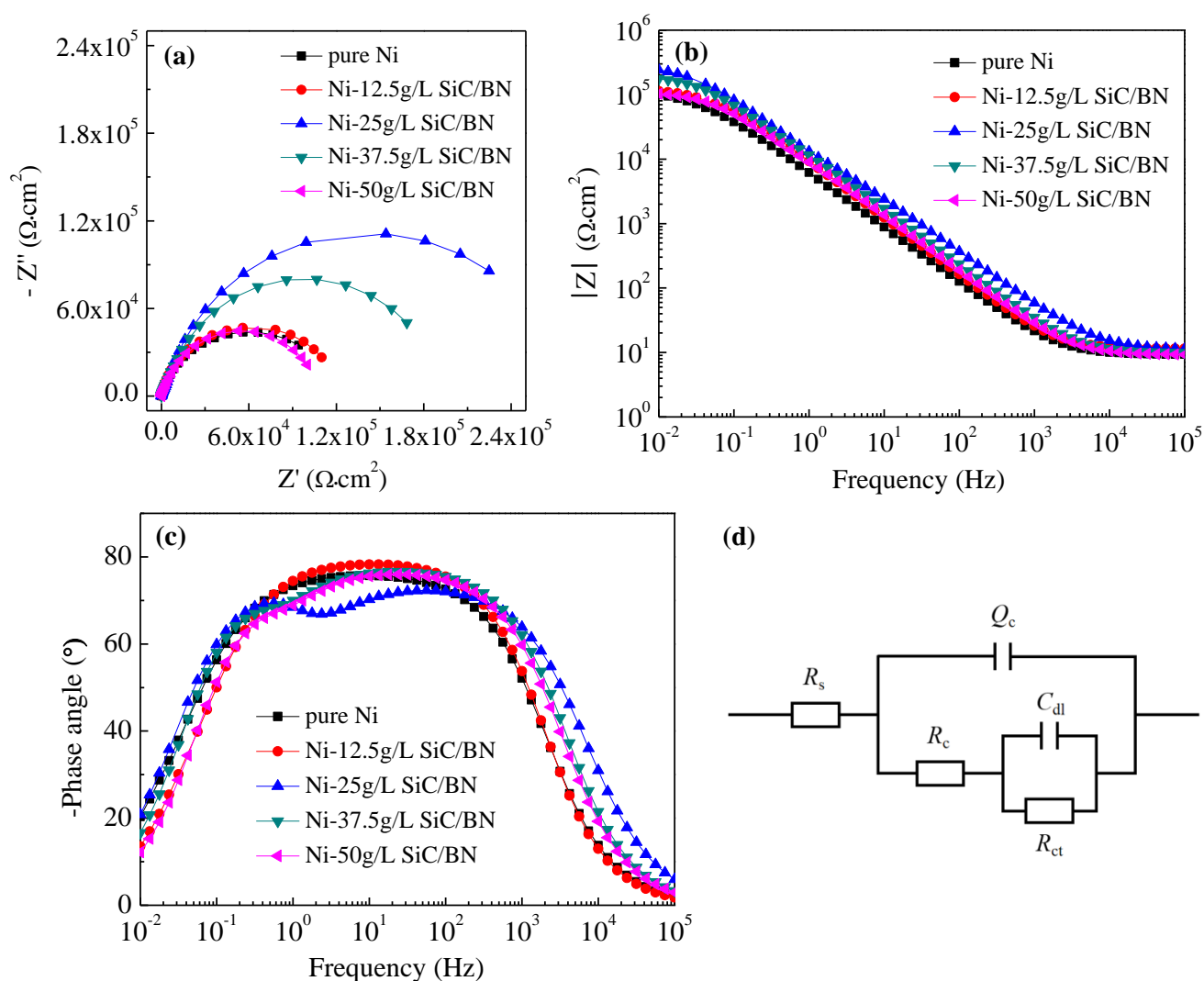


Figure 7. Nyquist plot (a), Bode plot (b-c) and equivalent circuit model (d) showing the corrosion process of pure Ni and Ni-SiC-BN composite coatings in 3.5 wt.% NaCl solution.

Table 1 Fitting results of EIS data obtained from coatings.

Samples	R_s ($\Omega \cdot \text{cm}^2$)	Q_c ($\text{F} \cdot \text{cm}^{-2} \cdot \text{s}^{n-1}$)	n	R_c ($\Omega \cdot \text{cm}^2$)	C_{dl} ($\text{F} \cdot \text{cm}^{-2}$)	R_{ct} ($\Omega \cdot \text{cm}^2$)
pure Ni	9.198	3.313×10^{-5}	0.8526	1.051×10^5	6.138×10^{-4}	1.351×10^4
Ni-12.5g/L SiC/BN	11.40	2.088×10^{-5}	0.8827	1.058×10^5	2.705×10^{-4}	1.631×10^4
Ni-25g/L SiC/BN	10.96	1.332×10^{-5}	0.8255	3.268×10^4	3.553×10^{-6}	2.518×10^5
Ni-37.5g/L SiC/BN	9.824	1.607×10^{-5}	0.8668	6.540×10^4	7.190×10^{-6}	1.290×10^5
Ni-50g/L SiC/BN	9.148	2.054×10^{-5}	0.8622	4.499×10^4	9.486×10^{-6}	6.449×10^4

4. CONCLUSIONS

In this work, the effects of SiC and BN concentration in the bath on the microstructure, microhardness and corrosion resistance of Ni–SiC–BN composite coating were investigated. The results can be summarized as follows:

(1) By SiC and BN particles addition to the bath, the grain size of the composite coating was decreased, whereas increased with the increase in the particles concentration. The content of these particles embedded in the composite coating increased until the particles concentration was 37.5 g/L. Ni–SiC–BN composite coatings with a compact and uniform microstructure, proper distribution of the particles were obtained at the particles concentration of 25 g/L and 37.5 g/L.

(2) The microhardness were increased significantly with the increase of the content of these particles embedded in the composite coating, which was related to the grain refinement, as well the strengthening effect of dispersed particles. The composite coating with the highest microhardness ($403.0 \pm 21.2 \text{ HV}_{0.2}$) was achieved at 37.5 g/L.

(3) By SiC and BN particles addition to the bath, the corrosion resistance was enhanced due to the compact and uniform microstructure. And these particles that act as a barrier limited the exposed area of Ni matrix to the corrosive medium. The composite coating with the maximum capacitance arc radius and R_{ct} value ($2.518 \times 10^5 \Omega \cdot \text{cm}^2$) was obtained at the particles concentration of 25 g/L, showing the highest corrosion resistance. Further increasing the particles concentration, the corrosion resistance of the composite coating was deteriorated.

ACKNOWLEDGEMENTS

This work was supported by Innovation Fund Project of Hebei University of Engineering [grant numbers SJ2101003008]; National Natural Science Foundation of China [grant number 51801051]; Key Research Project of Higher Education in Hebei Province [grant numbers ZD2021020, BJ2020029].

References

1. Q.W. Wang, J.L. Huang, J.N. Liu, Y.F. Yang, G.F. Han, W. Li, *Surf. Topogr–Metrol.*, 10 (2022) 015024.
2. S. Dehgahi, R. Amini, M. Alizadeh, *J. Alloy. Comp.*, 692 (2017) 622.
3. E. Pompei, L. Magagnin, N. Lecis, P.L. Cavallotti, *Electrochim. Acta*, 54 (2009) 2571.
4. N. Elkhoshkhany, A. Hafnway, A. Khaled, *J. Alloy. Comp.*, 695 (2017) 1505.

5. A.H. Noorbakhsh Nezhad, E. Mohammadi Zahrani, A.M. Alfantazi, *Corros. Sci.*, 197 (2022) 110095.
6. S.W. Jiang, L. Yang, J.N. Pang, H. Lin, Z.Q. Wang, *Surf. Coat. Tech.*, 286 (2016) 197.
7. R.Q. Li, Y.Y. Hou, B.X. Liu, D.A. Wang, J. Liang, *Electrochim. Acta*, 222 (2016) 1272.
8. T. Ratajski, I. Kalemba-Rec, P. Indyka, P. Ledwig, M.J. Szczerba, B. Dubiel, *Mater. Charact.*, 163 (2020) 110229.
9. B. Cai, Y.F. Tan, L. He, H. Tan, L. Gao, *Trans. Nonferrous Met. Soc. China*, 23 (2013) 1681.
10. M.Y. Cao, Y.H. Yue, X. Guo, B.J. Wang, *Int. J. Electrochem. Sci.*, 17 (2022) 220113.
11. N.S. Qu, D. Zhu, K.C. Chan, *Scripta Mater.*, 54 (2006) 1421.
12. Z.H. Chen, G.J. Shao, Z.P. Ma, J.J. Song, G.L. Wang, W.W. Huang, *Mater. Lett.*, 160 (2015) 34.
13. G. Parida, D. Chaira, M. Chopkar, A. Basu, *Surf. Coat. Tech.*, 205 (2011) 4871.
14. W.W. Chen, W. Gao, *Electrochim. Acta*, 55 (2010) 6865.
15. G. Hatipoglu, M. Kartal, M. Uysal, T. Cetinkaya, H. Akbulut, *Tribol. Int.*, 98 (2016) 59.
16. S.T. Aruna, C. Anandan, V.K.W. Grips, *Appl. Surf. Sci.*, 301 (2014) 383.
17. Y. Zhang, L.X. Wei, H.B. Zhang, J.D. Wang, C.Y. Ma, F.X. Xu, *J. Mater. Eng. Perform.*, 31 (2022) 602.
18. A.D. Torkamani, M. Velashjerdi, A. Abbas, M. Bolourchi, P. Maji, *J. Compos. Comp.*, 3 (2021) 106.
19. Z. Shahri, S.R. Allahkaram, A. Zarebidaki, *Appl. Surf. Sci.*, 276 (2013) 174.
20. G. Gyawali, H.S. Kim, K. Tripathi, T.H. Kim, S.W. Lee, *J. Mater. Sci. Tech.*, 30 (2014) 796.
21. N. Guglielmi, *J. Electrochem. Soc.*, 119 (1972) 1009.
22. C.T.J. Low, R.G.A. Wills, F.C. Walsh, *Surf. Coat. Tech.*, 201 (2006) 371.
23. W. Jiang, L.D. Shen, M.B. Qiu, X. Wang, M.Z. Fan, Z.J. Tian, *J. Alloy. Comp.*, 762 (2018) 115.
24. L. Benea, P.L. Bonora, A. Borello, S. Martelli, F. Wenger, P. Ponthiaux, J. Galland, *Solid State Ionics*, 151 (2002) 89.
25. M. Surender, R. Balasubramaniam, B. Basu, *Surf. Coat. Tech.*, 187 (2004) 93.
26. F.Y. Hou, W. Wang, H.T. Guo, *Appl. Surf. Sci.*, 252 (2006) 3812.
27. Z. Zhang, D.L. Chen, *Scripta Mater.*, 54 (2006) 1321.
28. R.Q. Li, Y.Y. Hou, J. Liang, *Appl. Surf. Sci.*, 367 (2016) 449.
29. Z. Mahidashti, M. Aliofkhazraei, N. Lotfi, *T. Indian I. Metals*, 71 (2018) 257.
30. Q.Y. Feng, T.J. Li, H.T. Teng, X.L. Zhang, Y. Zhang, C.S. Liu, J.Z. Jin, *Surf. Coat. Technol.*, 202 (2008) 4137.